Title

Brain signaling becomes less integrated and more segregated with age.

Journal

Network Neuroscience, 8(4)

Authors

Razban, Rostam
Antal, Botond
Dill, Ken
et al.

Publication Date

2024

DOI

10.1162/netn_a_00389

Peer reviewed

NETWORK NEUROSCIENCE

an open access journal

Citation: Razban, R. M., Antal, B. B., Dill, K. A., & Mujica-Parodi, L. R. (2024). Brain signaling becomes less integrated and more segregated with age. *Network Neuroscience*, *8*(4), 1051–1064. https://doi.org/10.1162/netn_a_00389

DOI:
https://doi.org/10.1162/netn_a_00389

Supporting Information:
https://doi.org/10.1162/netn_a_00389

Received: 17 November 2023
Accepted: 17 May 2024

Competing Interests: The authors have declared that no competing interests exist.

Corresponding Author:
Lilianne R. Mujica-Parodi
lilianne.strey@stonybrook.edu

Handling Editor:
Emma Towlson

The MIT Press

RESEARCH

Brain signaling becomes less integrated and more segregated with age

Rostam M. Razban[1], Botond B. Antal[2,3], Ken A. Dill[1,4,5], and Lilianne R. Mujica-Parodi[1,2,3,6]

[1]Laufer Center for Physical and Quantitative Biology, Stony Brook University, Stony Brook, NY, USA
[2]Department of Biomedical Engineering, Stony Brook University, Stony Brook, NY, USA
[3]Athinoula A. Martinos Center for Biomedical Imaging, Massachusetts General Hospital and Harvard Medical School, Boston, MA, USA
[4]Department of Physics and Astronomy, Stony Brook University, Stony Brook, NY, USA
[5]Department of Chemistry, Stony Brook University, Stony Brook, NY, USA
[6]Santa Fe Institute, Santa Fe, NM, USA

Keywords: Aging, fMRI, dMRI, Statistical physics

ABSTRACT

The integration-segregation framework is a popular first step to understand brain dynamics because it simplifies brain dynamics into two states based on global versus local signaling patterns. However, there is no consensus for how to best define the two states. Here, we map integration and segregation to order and disorder states from the Ising model in physics to calculate state probabilities, P_{int} and P_{seg}, from functional MRI data. We find that integration decreases and segregation increases with age across three databases. Changes are consistent with weakened connection strength among regions rather than topological connectivity based on structural and diffusion MRI data.

AUTHOR SUMMARY

The integration-segregation framework succinctly captures the trade-off that brains face between seamless function (more integration) in light of energetic constrains (more segregation). Despite its ubiquitous use in the field, there is no consensus on its definition with various graph theoretical properties being proposed. Here, we define the two states based on the underlying mechanism of neuronal coupling strength to provide a physical foundation for the framework. We find that younger adults' brains are close to perfectly balanced between integration and segregation, while older adults' brains veer off toward random signaling.

INTRODUCTION

Aging is the number one risk factor for almost all neurodegenerative diseases (Kennedy et al., 2014). For every 5 years after the age of 65, the probability of acquiring Alzheimer's disease doubles (Bermejo-Pareja et al., 2008). An influential conceptual approach to begin making sense of brain dynamics frames it in terms of a balance between integrated and segregated network states (Deco, Tononi, Boly, & Kringelbach, 2015; Friston, 2009; Sporns, 2010, 2013; Tononi, Sporns, & Edelman, 1994; Wig, 2017). On one hand, the brain faces functional pressure to have as many regions directly connected for quick communication. On the other

State:
A particular combination of physical properties. Here, we assume that brain networks can only occupy either the integrated or segregated state.

Integration:
A network state composed of global signaling.

Segregation:
A network state limited to local signaling.

hand, the brain is constrained to minimize metabolic energy consumption because it consumes 10 times more of the body's energy than expected by mass (Raichle, 2006). Tuning the balance between extensive global signaling, referred to as integration, and limited local signaling, referred to as segregation, optimally compromises between functional and energetic constraints (Bullmore & Sporns, 2012; Cohen & D'Esposito, 2016; Manza et al., 2020; Wang et al., 2021). Although these constraints remain throughout life, age related glucose hypometabolism disrupts their balance.

Previous research has found mixed aging results, depending on the metrics used to measure integration and segregation (Chan, Park, Savalia, Petersen, & Wig, 2014; Chen et al., 2021; Onoda & Yamaguchi, 2013; Zhang et al., 2021). Although most in the literature use the system segregation metric (Chan et al., 2014), no consensus exists surrounding integration. In general, the problem facing the integration-segregation framework is that there is no one way to define the two states. Many graph theoretical metrics could potentially be used (Rubinov & Sporns, 2010), and it is unclear why one should take precedence over the other, particularly when their aging outcomes are mutually inconsistent. Thus, there is a need to more fundamentally define integration and segregation to transform it from a proxy to a physical quantity.

Ising model:
A classic model in physics that was first applied to ferromagnetism. It includes pairwise interactions between binary spin states.

Phase:
Interchangeable with the word "state" for the purposes of this text.

Here, we provide a physical foundation for the framework by applying the mean-field Ising model to treat integration and segregation as physical two-phase systems like magnets and liquids. After demonstrating that the Ising model can capture global brain dynamics as measured by functional MRI (fMRI) once the effective number of nodes is properly set, we proceed to calculate probabilities of being in the integrated or segregated states and find that younger and older brains are bounded by optimal and random signaling, respectively. We then explore diffusion and structural MRI data to ask if the age-related changes in signaling are due to changes in topological network connectivity.

APPLYING THE ISING MODEL TO FMRI

We model human brain signaling patterns obtained from resting-state fMRI datasets. As in previous work (Weistuch et al., 2021), we capture those patterns with the Ising model, a widely used theoretical method for expressing macroscale behaviors in terms of interactions among many underlying microscale agents (Dill & Bromberg, 2010). We first transform the continuous fMRI data into a representation as discrete Ising spins via binarization of the data (Figure 1). That is, we reduce the state of the region as either −1 or 1 based on whether fMRI signaling is decreasing or increasing, respectively. Second, we calculate the synchrony by summing over all spins in a given time interval and dividing by the total number of spins (Figure 1). Synchronies are collected over the entirety of the scan to obtain a distribution. Based on the Ising model theory, the synchrony threshold delineating between integrated and segregated states is set such that $P_{int} = P_{seg} = 1/2$ at the Ising model's critical point (see the Methods section). P_{seg} is the probability that the brain is in the segregated state and is defined as the relative number of time points for which the absolute value of synchrony is less than the synchrony threshold (Figure 1). P_{int} is defined as the relative number of time points for which the absolute value of synchrony is greater than the synchrony threshold and trivially relates to P_{seg} because $P_{int} + P_{seg} = 1$.

Critical point:
The point where two phases coexist. In this text, it is where the synchrony distribution dramatically changes from bimodal (primarily integrated) to unimodal (primarily segregated).

RESULTS

The Number of Functionally Effective Brain Regions

Before proceeding to calculate P_{seg}, we first check whether the model can capture the experimental synchrony distributions. A mean-field Ising model only considering pairwise

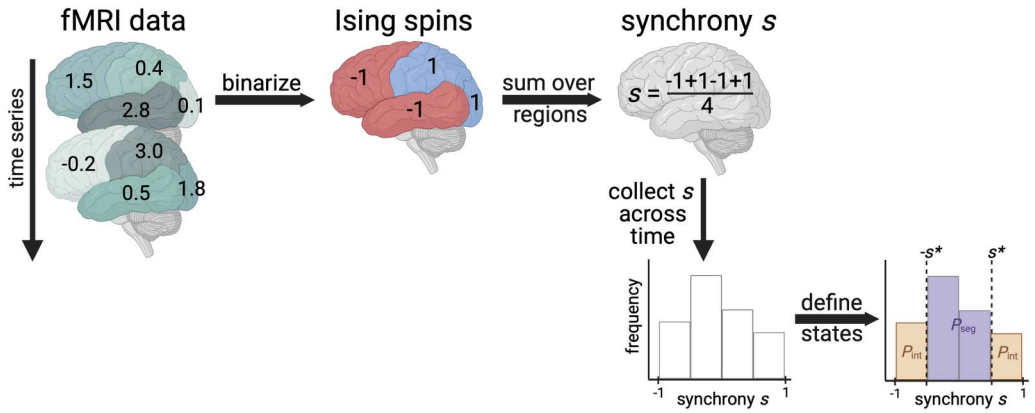

Figure 1. Calculating the probability that the brain exhibits integrated or segregated dynamics (P_{int} or P_{seg}). The schematic demonstrates the procedure for one individual's fictitious fMRI scan with four brain regions and only two time points shown. First, we binarize data based on the nearest neighbor scans in time. If the fMRI signal increases, a value of 1 is assigned; if it decreases, a value of −1 is assigned. Then, we calculate the average spin state of the brain, called synchrony. Finally, we collect synchrony values across the entire time series to create a synchrony distribution. We appropriately set the synchrony threshold based on the Ising model theory to delineate between integrated and segregated microstates. Additional details can be found in the Methods section. Figure was created with Biorender.com.

Principle of maximum entropy: A fitting strategy that satisfies user-defined constraints in the most agnostic way.

interactions has one quantity of interest, λ. The strength of connection λ between any two regions corresponds to the degree to which signals between any two brain regions are correlated. However, we find that a naive fit of λ based on the principle of maximum entropy (Dill & Bromberg, 2010; Schneidman, Berry, Segev, & Bialek, 2006; Weistuch et al., 2021) fails to capture the synchrony distribution from the fMRI data (Figure 2, orange). To improve upon a standard Ising model approach, here, we introduce a hyperparameter N_{eff}. Brain atlas parcellations provide N brain regions; however, those N regions must be identically distributed across time for the Ising model to apply. We find that when setting N to a lower value N_{eff}, fixed for all individuals within a dataset, the Ising model accurately captures synchrony distributions (Figure 2). The optimal value of $N_{eff} = 40$ is determined by scanning across N_{eff} multiples of 5 to find which best captures the next order moment not fit by our maximum entropy

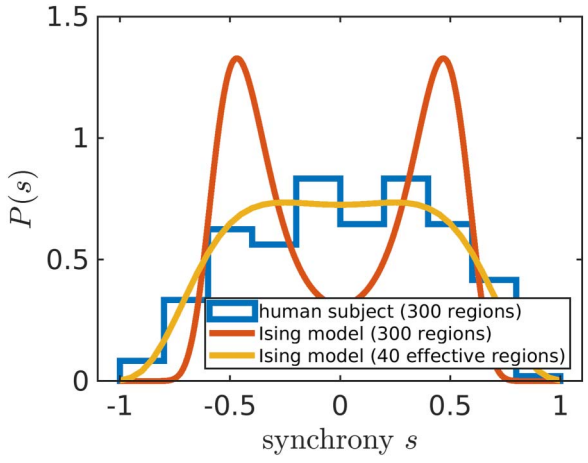

Figure 2. Adjusting the number of brain regions (N_{eff}) helps to reproduce the experimental data. The modified Ising model with $N_{eff} = 40$ (yellow line) better captures the synchrony distribution (blue histogram) of an arbitrarily chosen individual in the Cam-CAN dataset (subject ID: CC110045). The orange line corresponds to the Ising model with N equal to the number of regions in the Seitzman atlas (Seitzman et al., 2020).

setup across all individuals (see the Methods section; Figure 6). For our particular preprocessing (see the Methods section), we find that N_{eff} = 40 performs best for individuals in the Cambridge Centre for Ageing and Neuroscience (Cam-CAN) (Taylor et al., 2017) and the Human Connectome Project (HCP) Aging (Harms et al., 2018). For the UK Biobank (UKB) (Alfaro-Almagro et al., 2018), N_{eff} = 30 performs best (Figure 6).

Based on identified N_{eff} hyperparameter values, brains act as if they have a few tens of functional units. If different preprocessing decisions are considered, such as atlas resolution, N_{eff} values are still within an order of magnitude. At the voxel level (N = 125,879), we obtain an N_{eff} value of 65 for Cam-CAN and 125 for HCP using the same procedure as for the Seitzman atlas (N = 300) considered in the previous paragraph (Supporting Information Figure S2). Future work will pinpoint how N_{eff} depends on preprocessing to enable a future study creating a physics-based parcellation of the brain.

We also tried an alternative fitting strategy by fitting N_{eff} per individual rather than having the same value for all individuals in a respective dataset. We show that individually fitted N_{eff} values trivially relate to λ as expected by theory (Supporting Information Figure S1). Moreover, individually fitted N_{eff} are not found to be related to global differences in anatomical brain connectivity (Supporting Information Figure S3).

The Aging Brain Becomes Functionally More Segregated

With an appropriately determined N_{eff}, we can accurately set the same synchrony threshold s for all individuals within a dataset to calculate P_{seg}. The value of s^* is set such that at the Ising model's critical point in connection strength λ, P_{seg} equals to 1/2 for the ideal synchrony distribution based on the Ising model theory (see the Methods section). This enables P_{seg} comparisons across datasets that may have different N_{eff} values. For Cam-CAN and HCP, the value of s^* is s^* = 0.33 because N_{eff} = 40 for both datasets. For UKB, s^* = 0.36 (Supporting Information Table S1).

Across the three publicly available datasets, we find that the balance shifts toward more segregation at older ages (Figure 3). Note that if we plotted P_{int} rather than P_{seg}, Figure 3 would

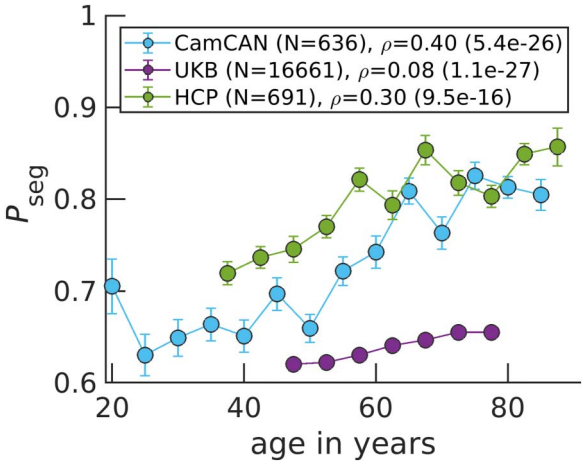

Figure 3. P_{seg} rises in aging brains across the three datasets. Data points correspond to medians, while error bars correspond to standard errors for bins of 5 years. The variable ρ corresponds to the Spearman correlation coefficient between age and P_{seg} calculated over all N individuals, with the p value in parenthesis.

be horizontally flipped, where P_{int} goes from high to low values as a function of increasing age because $P_{seg} + P_{int} = 1$. There is a large variation among the subjects (Supporting Information Figure S4). However, the correlation between age and P_{seg} is significant with the largest coefficient being 0.40 for Cam-CAN, while the lowest being 0.08 for UKB. Discrepancies in study designs may explain correlation magnitude differences: Cam-CAN and HCP are designed to study healthy aging (Bookheimer et al., 2019; Shafto et al., 2014), while the goal of UKB is to identify early biomarkers for brain diseases (Sudlow et al., 2015).

To better highlight how P_{seg} changes across Cam-CAN's large age range, we present violin plots for younger, middle age, and older individuals' P_{seg} (Supporting Information Figure S5). We also investigate how P_{seg} varies across time for a given individual. In Supporting Information Figure S6, we show that per individual P_{seg}, standard deviations decrease across age for Cam-CAN and HCP individuals. Finally, we perform a multiple linear regression with sex and handedness as additional covariates and show that age still strongly explains increasing segregation (Supporting Information Tables S2–S4 and Figures S7–S9).

Informed by the Ising model, increases in segregation result from network reorganization to more local signaling because of weakened connection strength between regions. Interestingly, younger individuals exhibit segregation behavior closer to the Ising model's critical point of connection strength (Supporting Information Figure S10). At the critical point, we define $P_{seg} = 1/2$ (see the Methods section) and find experimental P_{seg} values closer to 1/2 for younger individuals (Figure 3). Older individuals, on the other hand, approach $P_{seg} = 1$ on average. This limit corresponds to functionally uncoupled brain regions that are randomly activating. Our results support the critical brain hypothesis that healthy brains operate near a critical point (Beggs, 2022; Beggs & Plenz, 2003; Ponce-Alvarez, Kringelbach, & Deco, 2023; Tagliazucchi, Balenzuela, Fraiman, & Chialvo, 2012) and implicate aging as pushing brain dynamics further away from criticality.

Increasing Segregation Is Not Related to Structural Degradation

In the previous subsection, we discussed the disruption of the integration and segregation balance from the perspective of phase transitions in physics. Here, we explore the physiological mechanism underlying increasing segregation in the aging brain. We consecutively simulate the Ising model on a hypothetically degrading brain structure and show that random removal of edges yields qualitatively similar results to those of fMRI (Figure 4). Note that Figure 4 is horizontally flipped from that of P_{seg} (Figure 3) because the average degree (relative number of edges) is on the *x*-axis. It is presumed that edges are lost as age increases. In Figure 4, edges are lost linearly in time; however, more complicated monotonic functions can be employed to yield a quantitative match with experimental data in Figure 3. We can also capture variability among individuals by assuming that connection strengths within an individual are drawn from a distribution, rather than all being equal (Supporting Information Figure S11). In the Supporting Information, we also demonstrate that similar qualitative trends are obtained when starting with other individuals' structures, regardless of their age (Supporting Information Figure S12).

We now begin to investigate possible mechanisms of connection degradation. First, we find that our simulation is agnostic to the detailed mechanism of connection degeneration because connection strength is essentially modulated by the probability that a given edge exists (Supporting Information Figure S13). In other words, the simulation cannot inform whether connections are degraded based on some targeted property. Thus, we turn to structural MRI and diffusion MRI data from UKB to investigate possible properties being degraded with age. In Supporting Information Figure S15, we confirm that white matter volume decreases as a

White matter:
Bundles of axons connecting brain regions.

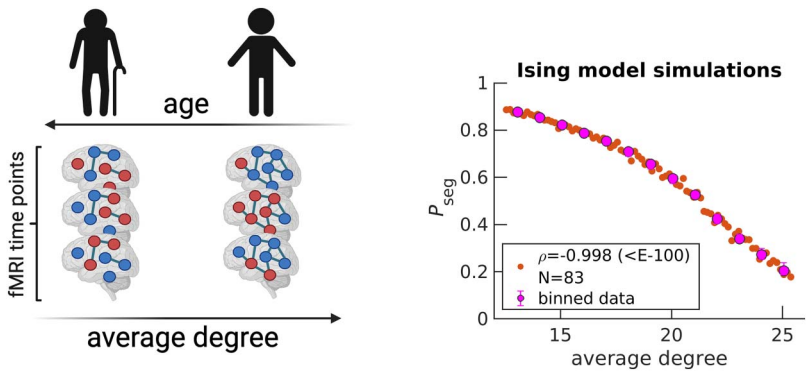

Figure 4. Simulating the random removal of edges results in P_{seg} increases. Five edges are randomly removed from a starting diffusion MRI structure (arbitrarily chosen UKB individual, subject ID: 6025360, 51 years old), under the Harvard-Oxford atlas (64 regions). An Ising system is simulated with $N_{eff} = N = 64$ for the corresponding diffusion MRI structure. Spin states, denoted by dark blue and red node colors in the schematic, are recorded across 2,500 time steps to calculate P_{seg}. Then, the entire procedure is repeated for the updated structure after edge removal, for a total of 83 times (see the Methods section). Orange data points on the right plot correspond to individual Ising systems, where N reflects the total number. The variable ρ corresponds to the Spearman correlation coefficient calculated over all orange data points between average degree and P_{seg}, with the p value in parenthesis. Magenta data points correspond to medians, while error bars correspond to upper and lower quartiles for bin sizes of one degree. The schematic on the left is created with Biorender.com.

function of adult age, as previously reported (Bethlehem et al., 2022; Lawrence et al., 2021; Lebel et al., 2012). However, this decrease does not correspond to a loss of anatomical connections because we find that neither average degree, average tract length, nor average tract density monotonically decrease with age when analyzing diffusion MRI scans using the Q-Ball method (Supporting Information Figure S16). This seems to contradict previous findings, which report decreases (Betzel et al., 2014; Lim, Han, Uhlhaas, & Kaiser, 2015). However, previous results employed the more simple diffusion tension imaging (DTI) method, which is known to be less accurate at performing tractography (Garyfallidis et al., 2014; Jones, Knösche, & Turner, 2013; Rokem et al., 2015). When rerunning our analysis for DTI, we can reproduce previously reported tract properties' anticorrelations with age (Supporting Information Figure S16). We also investigate a graph property that captures polysynaptic connectivity called communicability (Andreotti et al., 2014; Estrada & Hatano, 2008; Seguin, Sporns, & Zalesky, 2023) and find that it also does not decrease age when using Q-Ball-derived tract density (Supporting Information Figure S17).

We propose that observed white matter volume reduction (Supporting Information Figure S15) and brain dynamics change correspond to less myelin covering axons as functions of age. Despite rejecting anatomical connections as a possible mechanism in the previous paragraph, it remains inconclusive whether myelin underlies trends because we are not aware of such data being publicly available. Although axons are still physically present, myelin coverage disruption causes regions to no longer be functionally connected because signals do not arrive on time. Previously reported results from myelin water imaging confirm reduction in myelin at advanced ages (Arshad, Stanley, & Raz, 2016; Buyanova & Arsalidou, 2021). We also investigated whether degraded functional connections are likely to be longer than average with age, as previously reported for certain brain regions (Tomasi & Volkow, 2012). Although we indeed find that the average correlation of the 25% longest connections is slightly more strongly anti-

correlated with age compared with the average correlation of the 25% shortest connections for Cam-CAN (Supporting Information Figure S18, left), we find the opposite trend for HCP (Supporting Information Figure S18, right). Thus, myelin reduction does not seem to have a stronger impact on longer connections and conclude that the loss of functional connections happens randomly with respect to length at the brain-wide scale.

DISCUSSION

We apply the mean-field Ising model to physically quantify integration and segregation at the emergent scale of the whole brain. From resting-state fMRI scans across three publicly available datasets, we find that brain dynamics steadily becomes more segregated with age. Physically, aging leads to brain dynamics moving further away from its optimal balance at the critical point. Physiologically, analyses of white matter properties point to random functional connection losses due to myelin degeneration as the possible culprit for more segregated dynamics. This expands upon our previous work finding metabolic dysfunction to underly brain aging (Weistuch et al., 2021), hinting that myelin may be especially vulnerable to energy imbalance.

The Ising model and integration-segregation frameworks are considered as the simplest approaches to capture dynamics in their respective fields. Thus, it is fitting to map segregated and integrated states in neuroscience to disordered and ordered Ising model phases in physics, respectively. One general challenge in applying graph theory to MRI-level data is identifying what constitutes a node (DeFelipe, 2010; Lacy & Robinson, 2020; Seung, 2012; Sporns, 2010; Wig, Schlaggar, & Petersen, 2011; Yeo & Eickhoff, 2016). We identify the best number of effective brain regions N_{eff} such that the Ising model accurately captures individuals' synchrony distributions across the corresponding dataset, improving upon our original application of the Ising model, which lacked the N_{eff} hyperparameter (Weistuch et al., 2021). Future work will utilize N_{eff} calculations to guide the creation of a parcellation in which brain regions are constrained to be physically independent based on their collective functional activity.

The field is inundated with integration and segregation metrics that have different aging trends. We go beyond heuristic definitions, such as one that we previously proposed based on matrix decomposition (Weistuch et al., 2021), by self-consistently defining the two states within the Ising model framework. This makes our metric mechanistically based on the connection strength between regions and further stands out because P_{seg} and P_{int} are naturally at the emergent scale of the brain. Notably, we do not calculate a local property and then average over nodes to yield a brain-wide value (Wang et al., 2021's metric also has this advantage). In addition, P_{seg} and P_{int} are directly related because $P_{\text{seg}} + P_{\text{int}} = 1$. Most integration and segregation metrics (Chan et al., 2014; Rubinov & Sporns, 2010; Tononi et al., 1994; Wang et al., 2021) are not defined to be anticorrelated. This could be advantageous because greater complexity can be captured (Sporns, 2010).

Taken together, it is not surprising that P_{seg} and P_{int} results are not consistent with some previous aging reports. For example, a property called system segregation, defined as the difference between inter- and intracorrelations among modules, was found to decrease with age (Chan et al., 2014). Although most report that segregation decreases with age, regardless of the specific metric (Chan et al., 2014; Damoiseaux, 2017; King et al., 2018; Zhang et al., 2021; see Chen et al., 2021 for an exception), integration trends are less clear. Global efficiency, taken from the graph theory, was found to increase with age (Chan et al., 2014; Yao et al., 2019); however, others found different integration metrics decreasing with age (Chong et al.,

2019; Oschmann, Gawryluk, & The Alzheimer's Disease Neuroimaging Initiative, 2020; Zhang et al., 2021), consistent with the results reported here.

The utility of the integration-segregation framework lies in its simplicity. However, its simplicity has led to various heuristic definitions that have qualitatively different aging trends. By physically defining integration and segregation based on connection strength between regions, we provide an interpretable foundation for more detailed studies going beyond the two-state approximation to investigate brain dynamics.

METHODS

Functional MRI Preprocessing

We access three publicly available resting-state fMRI datasets: Cam-CAN (Taylor et al., 2017), UKB (Alfaro-Almagro et al., 2018), and HCP (Harms et al., 2018). Acquisition details such as the field strength and repetition time can be found in Supporting Information Table S5. Demographic details can be found in Supporting Information Table S6.

UKB and HCP fMRI data are accessed in preprocessed form (for details, see Alfaro-Almagro et al., 2018, and Glasser et al., 2013, 2018, respectively). We preprocessed Cam-CAN data as done in our previous work (Weistuch et al., 2021). For all three datasets, the cleaned, voxel space time series are band-pass filtered to only include neuronal frequencies (0.01–0.1 Hz) and smoothed at a full width at half maximum of 5 mm. Finally, we parcellate into 300 regions of interest according to the Seitzman atlas (Seitzman et al., 2020). For our voxel-wide analysis presented in the Supporting Information, we do not perform parcellation and just consider gray mater voxels by masking.

Applying the Ising model requires the data to only take two possible values: −1 or 1. After performing the preprocessing outlined in the previous paragraph, we binarize the continuous signal for a given region based on the sign of the slope of subsequent time points (Weistuch et al., 2021). We previously showed that such binarization still yields similar functional connectivities as that of the continuous data (Weistuch et al., 2021).

Finally, we only consider brain scans that have the same number of measurements as the predominant number of individuals in the respective dataset (Supporting Information Table S5). If the fitted connection strength parameter λ is less than 0, reflecting a nonphysical value, we do not include that individual's brain scan in our analysis. In the HCP dataset, we excluded individuals aged 90 years or older because their exact age, considered protected health information, is not available.

Identifying the N_{eff} Hyperparameter

In Figure 2, our maximum entropy fit (orange line) fails to qualitatively capture the synchrony distribution for an arbitrary individual. To rescue the fit, we replace N with N_{eff} (Supporting Information Equation S1). In the right plot of Figure 5, we demonstrate that a mean-field Ising model with $N_{\text{eff}} = 40$ accurately captures the fourth moment of synchrony $\langle s^4 \rangle$ across all individuals in Cam-CAN preprocessed under the Seitzman atlas. Note that N_{eff} is not a parameter like λ; rather, it is a hyperparameter because it takes the same value across all individuals within the dataset. N_{eff} is necessary because the Ising model systematically underestimates $\langle s^4 \rangle$ when $\Lambda > 0$ (left plot of Figure 5). Note that Λ corresponds to rescaling λ such that $\Lambda = 0$ is at the critical point (Supporting Information Equation S13).

To identify $N_{\text{eff}} = 40$ as the best value, we perform a parameter scan over multiples of 5 and identify the N_{eff} at which the root mean square error (RMSE) between $\langle s^4 \rangle_{\text{exp}}$ and $\langle s^4 \rangle_{\text{model}}$ is

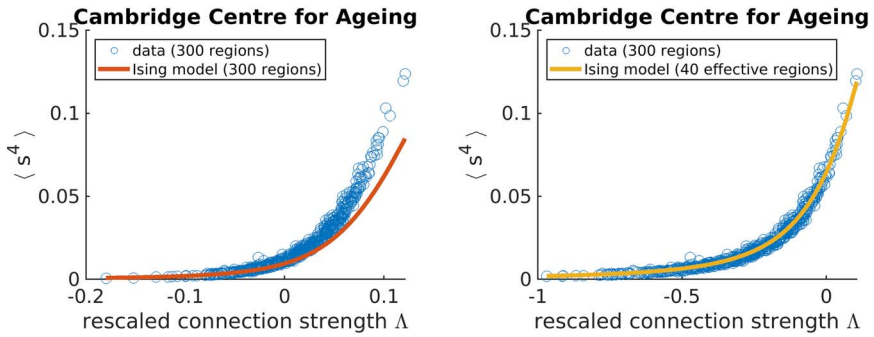

Figure 5. Adjusting the effective number of brain regions (N_{eff}) helps capture synchrony distributions' variances across individuals in the Cambridge Centre for Ageing data set. Each data point corresponds to an individual.

minimized (Figure 6). We choose the fourth moment because it is the next order moment that our maximum entropy fit does not constrain. It is not the third moment because the distribution is assumed to be an even function as indicated by our prior (Supporting Information Equation S1).

Calculating P_{seg}

The probability of the brain network being in the segregated state is the sum over all microstates corresponding to the segregated state.

$$P_{\text{seg}} = \sum_{n=-N_{\text{eff}}s^*}^{N_{\text{eff}}s^*} P(n) \tag{1}$$

$$P_{\text{seg}} = \frac{1}{Z} \sum_{n=-N_{\text{eff}}s^*}^{N_{\text{eff}}s^*} \binom{N_{\text{eff}}}{(N_{\text{eff}}+n)/2} e^{\lambda n^2/N_{\text{eff}}^2} \tag{2}$$

In the second line, the mean-field Ising model's $P(n)$ is inserted (Supporting Information Equation S2). Z corresponds to the partition function and ensures that $P(n)$ is normalized. The constant s^* is the synchrony threshold for which segregated and integrated microstates are delineated. We set s^* such that $P_{\text{seg}} = 1/2$ when $\Lambda = 0$ according to theory. More specifically, we numerically calculate $P_{\text{seg}}(\Lambda = 0)$ for a given N_{eff} and extrapolate to find s^* (Supporting Information Figure S19). Proper calibration ensures that the theory is accurate and enables apples to apples P_{seg} comparisons across datasets with different N_{eff}. The list of s^* values for the three publicly available datasets studied can be found in Supporting Information Table S1.

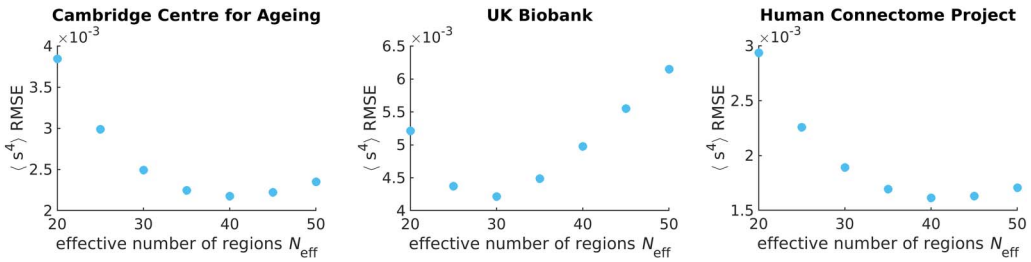

Figure 6. The effective number of regions N_{eff} is identified by minimizing the root mean square error (RMSE) of the fourth moment of synchrony between theory and experiment across all individuals. Each data point corresponds to the sum over all individuals' RMSEs in the respective data set. Note that the y-axis should be scaled by 10^{-3}.

Ising Model Simulation

We simulate the Ising model on an initial structure informed by diffusion MRI under the Harvard-Oxford atlas (Makris et al., 2006) (64 regions) for an arbitrarily chosen UKB individual (subject ID: 6025360). If no edge exists between two regions, then the regions are uncoupled. If an edge does exist, then regions i and j are coupled and contribute $\lambda * \sigma_i * \sigma_j$ to the system's energy, where λ corresponds to the connection strength and σ corresponds to the spin state of the corresponding region (−1 or 1). Under the standard notation of the Ising model, $\lambda = J/T$, where J corresponds to the coupling constant and T is the temperature of the bath. The starting λ is set to 34.4, which is above λ's critical point (starting $P_{seg} \approx 0.2$). By definition, $N_{eff} = N = 64$ in the simulations. Based on the atlas resolution, simulating the Harvard-Oxford atlas provides an N_{eff} similar to those found for the experimental data (N_{eff} = 40 for Cam-CAN and HCP; N_{eff} = 30 for UKB).

The simulation for a given structure starts by randomly assigning the 64 nodes up or down spins. Then, for each time step, we attempt 10 spin flips 64 times, for a total of 2,500 time steps. Spin flips are accepted according to the Metropolis-Hastings algorithm (Metropolis, Rosenbluth, Rosenbluth, Teller, & Teller, 1953). The exact number of spin flip attempts or total time points does not matter, as long as equilibrium is reached. For example, we find that for λ values larger than those presented in the text, synchrony distributions become asymmetric and exhibit only one of the two peaks corresponding to the integrated state because of the high kinetic barrier of going from all down spins to all up spins.

Although the starting structure is informed by diffusion MRI (dMRI), resulting structures after computational edge removals are based on the posited removal strategy. Edges informed by dMRI are undirected and removal maintains undirectedness. Effectively two times as many edges are removed because both forward and backward edges are concurrently eliminated. In Supporting Information Figure S14, we demonstrate how synchrony distributions change as edges are computationally removed for a UKB individual (subject ID: 6025360), with a starting λ = 34.4.

We also investigate other individuals' structures in the UKB to test the robustness of our qualitative results. We arbitrarily chose the following six individuals to widely sample different ages: subject IDs 6025360 (51 years old), 4712851 (57 years old), 3081886 (61 years old), 1471888 (65 years old), 4380337 (72 years old), and 1003054 (74 years old) (Supporting Information Figure S12). To ensure that the starting λ are comparable despite differing in the probability that two regions are connected (p_{edge}), we set λ_0 = 86.0 for all simulations such that $\lambda = \lambda_0 * p_{edge}$. For example, for subject ID 6025360, p_{edge} = 0.40, thus, the starting λ = 34.4.

Diffusion MRI Processing

Diffusion MRI processing to obtain structural information such as tract length and streamline count, which we call tract density, is outlined in our previous work (Razban, Pachter, Dill, & Mujica-Parodi, 2023). Briefly, we take preprocessed dMRI scans from the UKB (Sudlow et al., 2015) and calculate connectivity matrices using the Diffusion Imaging in the Python software (Garyfallidis et al., 2014). We input the Talairach atlas (Lancaster et al., 2000) to distinguish between white and gray matter. We perform deterministic tractography and reconstruct the orientation distribution function using Constant Solid Angle (Q-Ball) with a spherical harmonic order of 6 (Aganj et al., 2010). For Supporting Information Figure S16, we also do reconstruction using diffusion tensor imaging (Garyfallidis et al., 2014). To generate the starting structure for Ising model simulations, we input the Harvard-Oxford atlas for tractography because it parcellates the brain into fewer regions, making it more computationally tractable to carry out simulations, and is closer to N_{eff} values found for experimental data.

ACKNOWLEDGMENTS

We thank Ying-Jen Yang, Anthony Chesebro, Charles Kocher, Jonathan Pachter, and Lakshman Verma for insightful discussions. The research described in this paper is funded by the White House Brain Research Through Advancing Innovative Technologies Initiative (NSFNCS-FR 1926781 to L.R.M.-P. and K.A.D.) and the Stony Brook University Laufer Center for Physical and Quantitative Biology (K.A.D.). Data collection and sharing for this project was provided by the Cam-CAN. Cam-CAN funding was provided by the UK Biotechnology and Biological Sciences Research Council (grant number BB/H008217/1), together with support from the UK Medical Research Council and University of Cambridge, UK. This research has been conducted using the UKB Resource under Application Number 37462. Research reported in this publication was supported by the National Institute On Aging of the National Institutes of Health under Award Number U01AG052564 and by funds provided by the McDonnell Center for Systems Neuroscience at Washington University in St. Louis. The HCP-Aging 2.0 Release data used in this report came from DOI: 10.15154/1520707. The HCP data repository grows and changes over time. The HCP data used in this report came from NIMH Data Archive DOI: 10.15154/1526427.

SUPPORTING INFORMATION

Supporting information for this article is available at https://doi.org/10.1162/netn_a_00389. The following references are cited in the supporting information: Friedli and Velenik (2017), Kochmański et al. (2013), and Landau (1937).

AUTHOR CONTRIBUTIONS

Rostam M. Razban: Conceptualization; Data curation; Formal analysis; Investigation; Methodology; Visualization; Writing – original draft; Writing – review & editing. Botond B. Antal: Conceptualization; Data curation; Investigation; Software; Writing – original draft; Writing – review & editing. Ken A. Dill: Funding acquisition; Investigation; Methodology; Writing – original draft; Writing – review & editing. Lilianne R. Mujica-Parodi: Funding acquisition; Supervision; Visualization; Writing – original draft; Writing – review & editing.

FUNDING INFORMATION

Lilianne Mujica-Parodi, Division of Information and Intelligent Systems (https://dx.doi.org/10.13039/100000145), Award ID: 1926781.

CODE AND DATA AVAILABILITY

Scripts necessary to reproduce figures and conclusions reached in the text can be found at github.com/lcneuro/2state_brain. Please refer to the respective publicly available dataset to access previously published data (Cam-CAN, UKB, and HCP) (Alfaro-Almagro et al., 2018; Harms et al., 2018; Taylor et al., 2017).

REFERENCES

Aganj, I., Lenglet, C., Sapiro, G., Yacoub, E., Ugurbil, K., & Harel, N. (2010). Reconstruction of the orientation distribution function in single- and multiple-shell q-ball imaging within constant solid angle. *Magnetic Resonance in Medicine*, *64*(2), 554–566. https://doi.org/10.1002/mrm.22365, PubMed: 20535807

Alfaro-Almagro, F., Jenkinson, M., Bangerter, N. K., Andersson, J. L. R., Griffanti, L., Douaud, G., ... Smith, S. M. (2018). Image processing and Quality Control for the first 10,000 brain imaging datasets from UK Biobank. *NeuroImage*, *166*, 400–424. https://doi.org/10.1016/j.neuroimage.2017.10.034, PubMed: 29079522

Andreotti, J., Jann, K., Melie-Garcia, L., Giezendanner, S., Abela, E., Wiest, R., ... Federspiel, A. (2014). Validation of network communicability metrics for the analysis of brain structural networks.

PLoS One, *9*(12), e115503. https://doi.org/10.1371/journal.pone.0115503, PubMed: 25549088

Arshad, M., Stanley, J. A., & Raz, N. (2016). Adult age differences in subcortical myelin content are consistent with protracted myelination and unrelated to diffusion tensor imaging indices. *NeuroImage*, *143*, 26–39. https://doi.org/10.1016/j.neuroimage.2016.08.047, PubMed: 27561713

Beggs, J. M. (2022). Addressing skepticism of the critical brain hypothesis. *Frontiers in Computational Neuroscience*, *16*, 703865. https://doi.org/10.3389/fncom.2022.703865, PubMed: 36185712

Beggs, J. M., & Plenz, D. (2003). Neuronal avalanches in neocortical circuits. *Journal of Neuroscience*, *23*(35), 11167–11177. https://doi.org/10.1523/JNEUROSCI.23-35-11167.2003, PubMed: 14657176

Bermejo-Pareja, F., Benito-León, J., Vega, S., Medrano, M. J., Román, G. C., & Neurological Disorders in Central Spain (NEDICES) Study Group. (2008). Incidence and subtypes of dementia in three elderly populations of central Spain. *Journal of the Neurological Sciences*, *264*(1–2), 63–72. https://doi.org/10.1016/j.jns.2007.07.021, PubMed: 17727890

Bethlehem, R. A. I., Seidlitz, J., White, S. R., Vogel, J. W., Anderson, K. M., Adamson, C., … Alexander-Bloch, A. F. (2022). Brain charts for the human lifespan. *Nature*, *604*(7906), 525–533. https://doi.org/10.1038/s41586-022-04554-y, PubMed: 35388223

Betzel, R. F., Byrge, L., He, Y., Goñi, J., Zuo, X.-N., & Sporns, O. (2014). Changes in structural and functional connectivity among resting-state networks across the human lifespan. *NeuroImage*, *102*, 345–357. https://doi.org/10.1016/j.neuroimage.2014.07.067, PubMed: 25109530

Bookheimer, S. Y., Salat, D. H., Terpstra, M., Ances, B. M., Barch, D. M., Buckner, R. L., … Yacoub, E. (2019). The lifespan Human Connectome Project in aging: An overview. *NeuroImage*, *185*, 335–348. https://doi.org/10.1016/j.neuroimage.2018.10.009, PubMed: 30332613

Bullmore, E., & Sporns, O. (2012). The economy of brain network organization. *Nature Reviews Neuroscience*, *13*(5), 336–349. https://doi.org/10.1038/nrn3214, PubMed: 22498897

Buyanova, I. S., & Arsalidou, M. (2021). Cerebral white matter myelination and relations to age, gender, and cognition: A selective review. *Frontiers in Human Neuroscience*, *15*, 662031. https://doi.org/10.3389/fnhum.2021.662031, PubMed: 34295229

Chan, M. Y., Park, D. C., Savalia, N. K., Petersen, S. E., & Wig, G. S. (2014). Decreased segregation of brain systems across the healthy adult lifespan. *Proceedings of the National Academy of Sciences*, *111*(46), E4997–E5006. https://doi.org/10.1073/pnas.1415122111, PubMed: 25368199

Chen, X., Necus, J., Peraza, L. R., Mehraram, R., Wang, Y., O'Brien, J. T., … Taylor, J.-P. (2021). The functional brain favours segregated modular connectivity at old age unless affected by neurodegeneration. *Communications Biology*, *4*(1), 973. https://doi.org/10.1038/s42003-021-02497-0, PubMed: 34400752

Chong, J. S. X., Ng, K. K., Tandi, J., Wang, C., Poh, J.-H., Lo, J. C., … Zhou, J. H. (2019). Longitudinal changes in the cerebral cortex functional organization of healthy elderly. *Journal of Neuroscience*, *39*(28), 5534–5550. https://doi.org/10.1523/JNEUROSCI.1451-18.2019, PubMed: 31109962

Cohen, J. R., & D'Esposito, M. (2016). The segregation and integration of distinct brain networks and their relationship to cognition. *Journal of Neuroscience*, *36*(48), 12083–12094. https://doi.org/10.1523/JNEUROSCI.2965-15.2016, PubMed: 27903719

Damoiseaux, J. S. (2017). Effects of aging on functional and structural brain connectivity. *NeuroImage*, *160*, 32–40. https://doi.org/10.1016/j.neuroimage.2017.01.077, PubMed: 28159687

Deco, G., Tononi, G., Boly, M., & Kringelbach, M. L. (2015). Rethinking segregation and integration: Contributions of whole-brain modelling. *Nature Reviews Neuroscience*, *16*(7), 430–439. https://doi.org/10.1038/nrn3963, PubMed: 26081790

DeFelipe, J. (2010). From the connectome to the synaptome: An epic love story. *Science*, *330*(6008), 1198–1201. https://doi.org/10.1126/science.1193378, PubMed: 21109663

Dill, K., & Bromberg, S. (2010). *Molecular driving forces: Statistical thermodynamics in biology, chemistry, physics, and nanoscience*. Garland Science. https://doi.org/10.4324/9780203809075

Estrada, E., & Hatano, N. (2008). Communicability in complex networks. *Physical Review E*, *77*(3), 036111. https://doi.org/10.1103/PhysRevE.77.036111, PubMed: 18517465

Friedli, S., & Velenik, Y. (2017). *Statistical mechanics of lattice systems: A concrete mathematical introduction*. Cambridge University Press. https://doi.org/10.1017/9781316882603

Friston, K. J. (2009). Modalities, modes, and models in functional neuroimaging. *Science*, *326*(5951), 399–403. https://doi.org/10.1126/science.1174521, PubMed: 19833961

Garyfallidis, E., Brett, M., Amirbekian, B., Rokem, A., van der Walt, S., Descoteaux, M., … Dipy Contributors. (2014). Dipy, a library for the analysis of diffusion MRI data. *Frontiers in Neuroinformatics*, *8*, 8. https://doi.org/10.3389/fninf.2014.00008, PubMed: 24600385

Glasser, M. F., Coalson, T. S., Bijsterbosch, J. D., Harrison, S. J., Harms, M. P., Anticevic, A., … Smith, S. M. (2018). Using temporal ICA to selectively remove global noise while preserving global signal in functional MRI data. *NeuroImage*, *181*, 692–717. https://doi.org/10.1016/j.neuroimage.2018.04.076, PubMed: 29753843

Glasser, M. F., Sotiropoulos, S. N., Wilson, J. A., Coalson, T. S., Fischl, B., Andersson, J. L., … WU-Minn HCP Consortium. (2013). The minimal preprocessing pipelines for the Human Connectome Project. *NeuroImage*, *80*, 105–124. https://doi.org/10.1016/j.neuroimage.2013.04.127, PubMed: 23668970

Harms, M. P., Somerville, L. H., Ances, B. M., Andersson, J., Barch, D. M., Bastiani, M., … Yacoub, E. (2018). Extending the Human Connectome Project across ages: Imaging protocols for the Lifespan Development and Aging projects. *NeuroImage*, *183*, 972–984. https://doi.org/10.1016/j.neuroimage.2018.09.060, PubMed: 30261308

Jones, D. K., Knösche, T. R., & Turner, R. (2013). White matter integrity, fiber count, and other fallacies: The do's and don'ts of diffusion MRI. *NeuroImage*, *73*, 239–254. https://doi.org/10.1016/j.neuroimage.2012.06.081, PubMed: 22846632

Kennedy, B. K., Berger, S. L., Brunet, A., Campisi, J., Cuervo, A. M., Epel, E. S., … Sierra, F. (2014). Geroscience: Linking aging to chronic disease. *Cell*, *159*(4), 709–713. https://doi.org/10.1016/j.cell.2014.10.039, PubMed: 25417146

King, B. R., van Ruitenbeek, P., Leunissen, I., Cuypers, K., Heise, K.-F., Santos Monteiro, T., … Swinnen, S. P. (2018). Age-related

declines in motor performance are associated with decreased segregation of large-scale resting state brain networks. *Cerebral Cortex*, *28*(12), 4390–4402. https://doi.org/10.1093/cercor/bhx297, PubMed: 29136114

Kochmański, M., Paszkiewicz, T., & Wolski, S. (2013). Curie–Weiss magnet—A simple model of phase transition. *European Journal of Physics*, *34*(6), 1555–1573. https://doi.org/10.1088/0143-0807/34/6/1555

Lacy, T. C., & Robinson, P. A. (2020). Effects of parcellation and threshold on brainconnectivity measures. *PLoS One*, *15*(10), e0239717. https://doi.org/10.1371/journal.pone.0239717, PubMed: 33002019

Lancaster, J. L., Woldorff, M. G., Parsons, L. M., Liotti, M., Freitas, C. S., Rainey, L., ... Fox, P. T. (2000). Automated Talairach atlas labels for functional brain mapping. *Human Brain Mapping*, *10*(3), 120–131. https://doi.org/10.1002/1097-0193(200007)10:3<120::AID-HBM30>3.0.CO;2-8, PubMed: 10912591

Landau, L. D. (1937). On the theory of phase transitions. I. *Zhurnal Eksperimental'noi i Teoreticheskoi Fiziki*, *11*, 19–32.

Lawrence, K. E., Nabulsi, L., Santhalingam, V., Abaryan, Z., Villalon-Reina, J. E., Nir, T. M., ... Thompson, P. M. (2021). Age and sex effects on advanced white matter microstructure measures in 15,628 older adults: A UK biobank study. *Brain Imaging and Behavior*, *15*(6), 2813–2823. https://doi.org/10.1007/s11682-021-00548-y, PubMed: 34537917

Lebel, C., Gee, M., Camicioli, R., Wieler, M., Martin, W., & Beaulieu, C. (2012). Diffusion tensor imaging of white matter tract evolution over the lifespan. *NeuroImage*, *60*(1), 340–352. https://doi.org/10.1016/j.neuroimage.2011.11.094, PubMed: 22178809

Lim, S., Han, C. E., Uhlhaas, P. J., & Kaiser, M. (2015). Preferential detachment during human brain development: Age- and sex-specific structural connectivity in diffusion tensor imaging (DTI) data. *Cerebral Cortex*, *25*(6), 1477–1489. https://doi.org/10.1093/cercor/bht333, PubMed: 24343892

Makris, N., Goldstein, J. M., Kennedy, D., Hodge, S. M., Caviness, V. S., Faraone, S. V., ... Seidman, L. J. (2006). Decreased volume of left and total anterior insular lobule in schizophrenia. *Schizophrenia Research*, *83*(2–3), 155–171. https://doi.org/10.1016/j.schres.2005.11.020, PubMed: 16448806

Manza, P., Wiers, C. E., Shokri-Kojori, E., Kroll, D., Feldman, D., Schwandt, M., ... Volkow, N. D. (2020). Brain network segregation and glucose energy utilization: Relevance for age-related differences in cognitive function. *Cerebral Cortex*, *30*(11), 5930–5942. https://doi.org/10.1093/cercor/bhaa167, PubMed: 32564073

Metropolis, N., Rosenbluth, A. W., Rosenbluth, M. N., Teller, A. H., & Teller, E. (1953). Equation of state calculations by fast computing machines. *Journal of Chemical Physics*, *21*(6), 1087–1092. https://doi.org/10.1063/1.1699114

Onoda, K., & Yamaguchi, S. (2013). Small-worldness and modularity of the resting-state functional brain network decrease with aging. *Neuroscience Letters*, *556*, 104–108. https://doi.org/10.1016/j.neulet.2013.10.023, PubMed: 24157850

Oschmann, M., Gawryluk, J. R., & The Alzheimer's Disease Neuroimaging Initiative. (2020). A longitudinal study of changes in resting-state functional magnetic resonance imaging functional connectivity networks during healthy aging. *Brain Connectivity*, *10*(7), 377–384. https://doi.org/10.1089/brain.2019.0724, PubMed: 32623915

Ponce-Alvarez, A., Kringelbach, M. L., & Deco, G. (2023). Critical scaling of whole-brain resting-state dynamics. *Communications Biology*, *6*(1), 627. https://doi.org/10.1038/s42003-023-05001-y, PubMed: 37301936

Raichle, M. E. (2006). The brain's dark energy. *Science*, *314*(5803), 1249–1250. https://doi.org/10.1126/science.1134405, PubMed: 17124311

Razban, R. M., Pachter, J. A., Dill, K. A., & Mujica-Parodi, L. R. (2023). Early path dominance as a principle for neurodevelopment. *Proceedings of the National Academy of Sciences*, *120*(16), e2218007120. https://doi.org/10.1073/pnas.2218007120, PubMed: 37053187

Rokem, A., Yeatman, J. D., Pestilli, F., Kay, K. N., Mezer, A., van der Walt, S., & Wandell, B. A. (2015). Evaluating the accuracy of diffusion MRI models in white matter. *PLOS ONE*, *10*(4), e0123272. https://doi.org/10.1371/journal.pone.0123272, PubMed: 25879933

Rubinov, M., & Sporns, O. (2010). Complex network measures of brain connectivity: Uses and interpretations. *NeuroImage*, *52*(3), 1059–1069. https://doi.org/10.1016/j.neuroimage.2009.10.003, PubMed: 19819337

Schneidman, E., Berry, M. J., II, Segev, R., & Bialek, W. (2006). Weak pairwise correlations imply strongly correlated network states in a neural population. *Nature*, *440*(7087), 1007–1012. https://doi.org/10.1038/nature04701, PubMed: 16625187

Seguin, C., Sporns, O., & Zalesky, A. (2023). Brain network communication: Concepts, models and applications. *Nature Reviews Neuroscience*, *24*(9), 557–574. https://doi.org/10.1038/s41583-023-00718-5, PubMed: 37438433

Seitzman, B. A., Gratton, C., Marek, S., Raut, R. V., Dosenbach, N. U. F., Schlaggar, B. L., ... Greene, D. J. (2020). A set of functionally-defined brain regions with improved representation of the subcortex and cerebellum. *NeuroImage*, *206*, 116290. https://doi.org/10.1016/j.neuroimage.2019.116290, PubMed: 31634545

Seung, S. (2012). *Connectome: How the brain's wiring makes us who we are*. HMH.

Shafto, M. A., Tyler, L. K., Dixon, M., Taylor, J. R., Rowe, J. B., Cusack, R., ... Cam-CAN. (2014). The Cambridge Centre for Ageing and Neuroscience (Cam-CAN) study protocol: A cross-sectional, lifespan, multidisciplinary examination of healthy cognitive ageing. *BMC Neurology*, *14*, 204. https://doi.org/10.1186/s12883-014-0204-1, PubMed: 25412575

Sporns, O. (2010). *Networks of the brain*. MIT Press. https://doi.org/10.7551/mitpress/8476.001.0001

Sporns, O. (2013). Network attributes for segregation and integration in the human brain. *Current Opinion in Neurobiology*, *23*(2), 162–171. https://doi.org/10.1016/j.conb.2012.11.015, PubMed: 23294553

Sudlow, C., Gallacher, J., Allen, N., Beral, V., Burton, P., Danesh, J., ... Collins, R. (2015). UK Biobank: An open access resource for identifying the causes of a wide range of complex diseases of middle and old age. *PLoS Medicine*, *12*(3), e1001779. https://doi.org/10.1371/journal.pmed.1001779, PubMed: 25826379

Tagliazucchi, E., Balenzuela, P., Fraiman, D., & Chialvo, D. R. (2012). Criticality in large-scale brain fMRI dynamics unveiled

by a novel point process analysis. *Frontiers in Physiology*, *3*, 15. https://doi.org/10.3389/fphys.2012.00015, PubMed: 22347863

Taylor, J. R., Williams, N., Cusack, R., Auer, T., Shafto, M. A., Dixon, M., ... Henson, R. N. (2017). The Cambridge Centre for Ageing and Neuroscience (Cam-CAN) data repository: Structural and functional MRI, MEG, and cognitive data from a cross-sectional adult lifespan sample. *NeuroImage*, *144*, 262–269. https://doi.org/10.1016/j.neuroimage.2015.09.018, PubMed: 26375206

Tomasi, D., & Volkow, N. D. (2012). Aging and functional brain networks. *Molecular Psychiatry*, *17*(5), 549–558. https://doi.org/10.1038/mp.2011.81, PubMed: 21727896

Tononi, G., Sporns, O., & Edelman, G. M. (1994). A measure for brain complexity: Relating functional segregation and integration in the nervous system. *Proceedings of the National Academy of Sciences*, *91*(11), 5033–5037. https://doi.org/10.1073/pnas.91.11.5033, PubMed: 8197179

Wang, R., Liu, M., Cheng, X., Wu, Y., Hildebrandt, A., & Zhou, C. (2021). Segregation, integration, and balance of large-scale resting brain networks configure different cognitive abilities. *Proceedings of the National Academy of Sciences*, *118*(23), e2022288118. https://doi.org/10.1073/pnas.2022288118, PubMed: 34074762

Weistuch, C., Mujica-Parodi, L. R., Razban, R. M., Antal, B., van Nieuwenhuizen, H., Amgalan, A., & Dill, K. A. (2021). Metabolism modulates network synchrony in the aging brain. *Proceedings of the National Academy of Sciences*, *118*(40), e2025727118. https://doi.org/10.1073/pnas.2025727118, PubMed: 34588302

Wig, G. S. (2017). Segregated systems of human brain networks. *Trends in Cognitive Sciences*, *21*(12), 981–996. https://doi.org/10.1016/j.tics.2017.09.006, PubMed: 29100737

Wig, G. S., Schlaggar, B. L., & Petersen, S. E. (2011). Concepts and principles in the analysis of brain networks. *Annals of the New York Academy of Sciences*, *1224*(1), 126–146. https://doi.org/10.1111/j.1749-6632.2010.05947.x, PubMed: 21486299

Yao, Z., Zou, Y., Zheng, W., Zhang, Z., Li, Y., Yu, Y., ... Hu, B. (2019). Structural alterations of the brain preceded functional alterations in major depressive disorder patients: Evidence from multimodal connectivity. *Journal of Affective Disorders*, *253*, 107–117. https://doi.org/10.1016/j.jad.2019.04.064, PubMed: 31035211

Yeo, B. T. T., & Eickhoff, S. B. (2016). A modern map of the human cerebral cortex. *Nature*, *536*(7615), 152–154. https://doi.org/10.1038/nature18914, PubMed: 27437585

Zhang, Y., Wang, Y., Chen, N., Guo, M., Wang, X., Chen, G., ... Hu, B. (2021). Age-associated differences of modules and hubs in brain functional networks. *Frontiers in Aging Neuroscience*, *12*, 607445. https://doi.org/10.3389/fnagi.2020.607445, PubMed: 33536893